Precision Engineering xxx (2013) xxx–xxx

Contents lists available at ScienceDirect

Precision Engineering

journal homepage: www.elsevier.com/locate/precision

# Large dynamic range nanopositioning using iterative learning control

Gaurav Parmar*, Kira Barton, Shorya Awtar

*Department of Mechanical Engineering, University of Michigan, 2350 Hayward Street, Ann Arbor, MI 48109, United States*

ARTICLE INFO

*Article history:*
Received 8 October 2012
Received in revised form 25 April 2013
Accepted 9 July 2013
Available online xxx

*Keywords:*
Large range nanopositioning
Iterative learning control
Dynamic range
Precision motion control

ABSTRACT

This paper presents the control system design and tracking performance for a large range single-axis nanopositioning system that is based on a moving magnet actuator and a flexure bearing. While the physical system is designed to be free of friction and backlash, the nonlinearities in the electromagnetic actuator as well as the harmonic distortion in the drive amplifier degrade the tracking performance for dynamic commands. It is shown that linear feedback and feedforward proves to be inadequate to overcome these nonlinearities. This is due to the low open-loop bandwidth of the physical system, which limits the achievable closed-loop bandwidth given actuator saturation concerns. For periodic commands, like those used in scanning applications, the component of the tracking error due to the system nonlinearities exhibits a deterministic pattern and repeats every period. Therefore, a phase lead type iterative learning controller (ILC) is designed and implemented in conjunction with linear feedback and feedforward to reduce this periodic tracking error by more than two orders of magnitude. Experimental results demonstrate the effectiveness of ILC in achieving 10 nm RMS tracking error over 8 mm motion range in response to a 2 Hz band-limited triangular command. This corresponds to a dynamic range of more than $10^5$ for speeds up to 32 mm/s, one of the highest reported in the literature so far, for a cost-effective desktop-sized single-axis motion system.

Published by Elsevier Inc.

## 1. Introduction and background

Nanopositioning is one of the key enabling technologies for measurement and manipulation of matter at the micro and nano scales [1]. Because of their nanometric (<10 nm) *motion quality* (accuracy, precision, and resolution), nanopositioning systems are employed in various sensitive applications that require relative scanning motion between a probe and a substrate. However, one of the main drawbacks of currently available nanopositioning systems is their small motion range of a few hundred microns per axis [2,3]. Increasing this range to several millimeters will enable large-size substrates in a number of applications such as scanning probe microscopy [4], scanning probe lithography [5], scanning beam lithography [6], and nanometrology [7].

The ongoing research efforts in the area of large range translational nanopositioning systems can be broadly classified into three categories. The first category is of positioning systems that have friction and backlash in one or more of their physical components, such as the bearing or transmission. The motion stage in these cases is supported by rolling [8–10] or sliding [11–13] guideways. Either direct-drive linear motors [9,12,13] or rotary motors coupled with lead-screw drives [8,10,11,14] are used for actuation. For these systems, linear feedback controllers do not offer adequate positioning performance due to the nonlinear and parameter-varying characteristics of friction, especially in the micro-dynamic regime [15]. Implementation of advanced controllers [8,10,13] has shown some performance improvements over linear feedback, especially for point-to-point positioning. However, achieving nanometric tracking performance for dynamic commands remains to be a challenge.

To overcome the performance limitations associated with friction, another approach has been to mount a small range, high motion quality positioning system (fine stage) on top of a large range, friction-based traditional motion system (coarse stage) [9,11,12,14]. The idea is to use the fine stage to compensate for the positioning errors of the coarse stage, thereby improving the overall positioning performance. The major challenge here, in achieving nanometric tracking performance, lies in the control system design to ensure coordination between the coarse and fine motion systems [14].

Separately, there has been a considerable effort focused on large range nanopositioning systems that are based on non-contact and frictionless operation. These systems rely on magnetic [16–18], aerostatic [19–22], or flexure bearings [2,23,24] for motion guidance, and generally employ direct-drive electromagnetic actuators. Each of these constructions presents unique control design challenges to achieve nanometric motion quality. For example, electromagnetic bearings and well as actuators suffer from force-stroke nonlinearities [17]. Additionally, the noise

* Corresponding author. Tel.: +1 7342392928.
*E-mail address:* parmar@umich.edu (G. Parmar).

0141-6359/$ – see front matter. Published by Elsevier Inc.
http://dx.doi.org/10.1016/j.precisioneng.2013.07.003

and distortion in the actuator driver degrades the positioning performance [24], also shown later in this paper. Air bearings exhibit sustained vibrations in both load-bearing as well as motion direction [25,26]. In case of flexure bearings, one of the major drawbacks has been their limited range of motion. Recent research [2,27] has shown up to 10 mm motion range in multi-axis flexure bearings, which is sufficient for intended applications. However, poorly damped high frequency poles and zeros in flexures limit the closed-loop performance [2]. Additionally, they require higher actuation effort to overcome the spring stiffness.

The motion quality of nanopositioning systems is dictated by the tracking error, which is the difference between the commanded and the measured position. Tracking error may be evaluated for either point-to-point positioning commands or for path-following commands. Point-to-point positioning is concerned with moving the motion stage from one point to another and staying there for some finite period of time. Only the final position is relevant and the path taken to reach that position is not. On the other hand, in the more general case of path-following, such as raster scanning, the motion stage is moved along a periodic trajectory in time and space, and position at each point along this trajectory is important. Obtaining nanometric tracking performance for such dynamic commands is relatively challenging because a linear controller may not provide adequate command following and disturbance rejection over a desired finite frequency range. While many of the above-mentioned references [2,8–10,16–18,20–24] have reported large range (>1 mm) and high resolution (<10 nm *Root Mean Square* or RMS) for point-to-point positioning commands, only a few have shown nanometric positioning performance for dynamic commands over a large motion range (Table 1). It should be noted that due to differences in the motion range, frequency content, and type of command trajectory used, it is not possible to compare the tracking performances of these systems in a consistent manner. However, it can be observed that the nanometric tracking performance is reported either over a small motion range or for slower or quasi-static commands.

Although lithographic steppers and scanners used in semiconductor manufacturing do provide large range and nanometric motion quality at relatively higher speeds [28], these machines are not targeted toward niche low-cost desktop applications mentioned before. Achieving such specifications in a cost-effective and desktop-sized setup is still a challenging problem, which is the focus of this paper.

In previous work [29], the design, fabrication, and testing of a single-axis nanopositioning system employing a flexure bearing and moving magnet actuator was presented. Point-to-point nanometric positioning performance was demonstrated over the entire motion range. However, nonlinearities associated with the actuator as well as the driver resulted in inadequate tracking performance in response to dynamic commands. In this paper, design and implementation of a classical feedback controller along with an iterative learning controller is presented to overcome these nonlinearities in order to achieve nanometric tracking performance for dynamic commands over a large motion range. In Section 2, the physical system is described along with its open-loop characterization. Next, in Section 3, it is shown that a linear feedback and feedforward controller by itself offers inadequate performance. This is because of the limited sensitivity reduction that is possible by employing a feedback loop, given actuator saturation and low open-loop bandwidth of the system. For scanning-type applications, in which the command is a periodic signal, the deterministic part of the error arising due to nonlinearities also repeats every period. This provides the motivation to employ iterative learning control (ILC) to reduce the repeating portion of the tracking error. Since its inception in early 1980s, ILC has seen tremendous applications in the fields of robotics [30] and motion systems [31,32]. Some of the advantages of ILC include its linear formulation, minimal knowledge of plant dynamics, simple design and implementation, and that fact that it can be applied to any existing feedback control system [30]. A brief introduction to ILC is presented in Section 4 followed by the design and implementation of a lead type ILC in conjunction with the existing feedback and feedforward controller. Experimental results, reported in Section 5, demonstrate more than two orders of magnitude reduction in the tracking error while following dynamic commands, when compared to the performance obtained with a linear feedback and feedforward controller only. Concluding remarks are presented in Section 6.

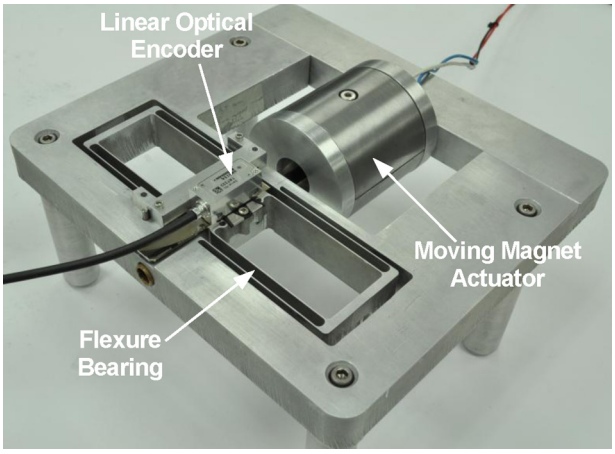


**Fig. 1.** Single-axis nanopositioning system.

## 2. Physical system description

The single-axis nanopositioning system prototype used in this work is shown in Fig. 1. This setup consists of a symmetric double parallelogram flexure bearing and a moving magnet actuator (MMA). A linear optical encoder (RELM scale, Si-HN-4000 read-head, and SIGNUM Interface from Renishaw) with 5 nm quantization steps is used for position measurement and feedback. The encoder read-head is mounted on the local ground of the flexure bearing and the scale is mounted on the motion stage. Hence, the sensor output is the relative displacement of the motion stage with respect to the local flexure ground. The physical construction of the system provides frictionless and backlash-free motion over a motion range of 8 mm. The detailed design and fabrication of the experimental setup can be found in [29]. A custom-made voltage amplifier (based on the MP111 power-OpAmp from Cirrus Logic) with a gain of 5 V/V and a bandwidth of 10 kHz is used to drive the MMA. The control system is implemented on a real-time hardware (DS1103 from DSpace) equipped with 16-bit digital-to-analog converter. While the sampling frequency and the loop rate are fixed at 10 kHz, all the measurements shown in this paper are taken at a bandwidth of 1 kHz.

In order to design a linear feedback controller, a linearized frequency domain model of the system is needed. Although, as mentioned later in this paper, there are known sources of nonlinearities in the system, they can be neglected for the purpose of obtaining a linearized plant model. The open-loop frequency response of the nanopositioning system was found experimentally via broadband FFT-based system identification technique. For this purpose, a chirp signal with a frequency content of 1–1000 Hz was sent as the input to the amplifier. The amplitude of the chirp signal was chosen to restrict the maximum displacement of the stage to be <10 μm. Next, the Matlab function *invfreqs* was used to fit a continuous-time stable transfer function, $P(s)$, to the open-loop frequency response,

Please cite this article in press as: Parmar G, et al. Large dynamic range nanopositioning using iterative learning control. Precis Eng (2013), http://dx.doi.org/10.1016/j.precisioneng.2013.07.003

**Table 1**
Dynamic tracking performance in large range nanopositioning systems.

| Reference | Motion range (mm) | Bearing | Actuator/transmission | Reference command | Tracking error (nm) |
|---|---|---|---|---|---|
| Buice et al. [11] | 50 | Linear guide (coarse), flexure (fine) | DC motor with leadscrew (coarse), PZT (fine) | 2.5 mm, 0.01 Hz sine | 45 |
| Choi et al. [12] | – | Linear guide (coarse), air bearing (fine) | Linear motor (coarse), voice coil (fine) | 20 mm/s constant velocity, 300 mm motion range | ±150 |
| Michellod et al. [14] | 70 | Flexure (coarse and fine) | Stepper motor with leadscrew (coarse), PZT (fine) | 10 μm, 200 Hz Kolmogorov signal | 8 (RMS) |
| Maeda et al. [21] | 10 | Air bearing | Voice coil | ±3 μm, 5 Hz band-limited triangular profile | ±5 |
| Zschaeck et al. [13] | 200 | Linear guide | Linear motor | 1 mm/s constant velocity, 10 mm motion range | 15 (RMS) |
| Fukada et al. [23] | 1 | Flexure | Moving magnet actuator | 0.125 mm/s constant velocity, 0.5 mm motion range | ±50 |
| Kim et al. [17] | 5 | Electromagnetic | Electromagnetic | 2.5 mm/s constant velocity, 5 mm motion range | 25 |
| This Paper | 10 | Flexure | Moving magnet actuator | ±4 mm, 2 Hz band-limited triangular profile | 10 (RMS) |

obtained using Fourier analysis of the collected input and output signals [33]. The resulting 5th order transfer function is given by

$$P(s) = \frac{1.28 \times 10^{10}(s^2 + 5.63s + 3.34 \times 10^5)}{(s + 333.1)(s^2 + 150.50s + 3.31 \times 10^4)(s^2 + 12.43s + 3.87 \times 10^5)} \quad (1)$$

Fig. 2 shows the experimentally obtained frequency response along with the frequency response of the estimated transfer function from the amplifier command to the measured position. The pole at 53 Hz corresponds to the electrical time constant of the actuator (44.3 Ω coil resistance and 133 mH coil inductance). The complex conjugate pole near 29 Hz corresponds to rigid body mode of the flexure bearing. The higher-order pole-zero pairs near 90 Hz is due to the resonance of the intermediate stages of the double-parallelogram flexure bearing. The damping seen in the rigid body mode is contributed by the eddy currents in the MMA aluminum coil bobbin as well as by the back-electromotive force dynamics. The open-loop bandwidth, defined as the frequency where the plant gain drops down by −3 dB, is approximately 35 Hz. The low open-loop bandwidth of the motion system is a consequence of the fundamental limitations arising from the physical design of MMA in flexure based motion systems [29].

Although the physical system described above is free of friction and backlash, the achievable positioning performance in the closed loop setup, shown in Fig. 3, is still limited by various factors described below:

1. Several sources of noise and disturbance that exist in the system limit the positioning resolution. This includes position sensor noise, actuator driver noise, electronic noise and quantization in the real-time control hardware, and mechanical floor vibrations.

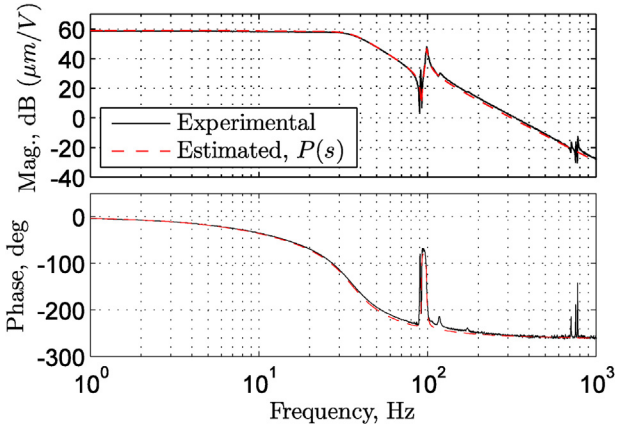


**Fig. 2.** Open-loop frequency response.

2. The force constant of the MMA is dependent on the position of the moving magnet with respect to the stator (coils and back-iron) [29]. This force-stroke nonlinearity, shown in Fig. 4, degrades the tracking performance.
3. The nonlinearity in the actuator driver also contributes to the tracking error. This nonlinearity shows up as the harmonic distortion at multiples of the fundamental excitation frequency of the command signal. Fig. 5 shows one such measurement of the power spectral density of the driver output, when the desired output is a 15 V, 2 Hz sinusoid. The signal-to-noise ratio, which is a measure of the broadband noise, is approximately 120 dB. However, the total harmonic distortion, defined as the ratio of power in the harmonics with respect to the power at the fundamental signal frequency, is about −90 dB. Since this nonlinearity is <0.01%, it is generally very difficult to model it accurately or further reduce it via circuit design.

## 3. Linear feedback design and limitations

A linear feedback controller is first implemented to achieve good command tracking as well as noise and disturbance rejection to overcome the abovementioned sources of errors. The estimated open-loop transfer function, $P(s)$ in Eq. (1), is used to design an internal model type linear feedback controller $C(s)$ using loop shaping technique. The controller consists of zeros to cancel the coil dynamics and well as the first resonance poles of the flexure. An integrator is added to ensure zero steady-state error and low frequency disturbance rejection. This is followed by high frequency damped poles to make the controller structure strictly proper in order to attenuate sensor noise amplification. The following compensator was implemented:

$$C(s) = \frac{1.57 \times 10^4(s + 141.5)(s^2 + 159.5s + 5.01 \times 10^4)}{s(s + 4000)(s^2 + 6700s + 1.92 \times 10^7)} \quad (2)$$

The frequency response of the analytical closed-loop transfer function, $T(s)$, along with the experimentally obtained closed-loop frequency response is shown in Fig. 6. The phase margin and gain margin of the loop transfer function are 43° and 9 dB, respectively. The effective bandwidth of the feedback loop, defined as the frequency where the sensitivity transfer function first crosses −3 dB from below, is approximately 85 Hz. The nanopositioning system was tested for its point-to-point positioning performance with step commands of 2 mm and 20 nm and the measured position response is shown in Fig. 7. The steady-state positioning error, which is a measure of the positioning resolution, is approximately 20–25 nm peak-to-peak or 4 nm RMS. Although the quantization step size of the linear optical encoder is 5 nm, the steady state peak-to-peak

Please cite this article in press as: Parmar G, et al. Large dynamic range nanopositioning using iterative learning control. Precis Eng (2013), http://dx.doi.org/10.1016/j.precisioneng.2013.07.003

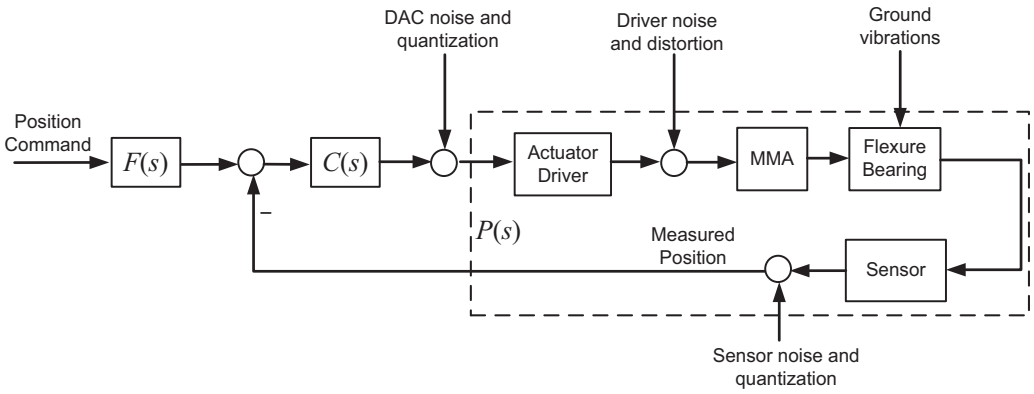


**Fig. 3.** Feedback architecture.

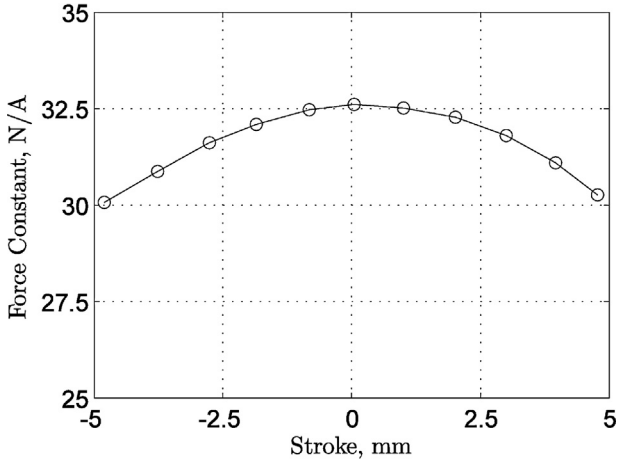


**Fig. 4.** MMA force-stroke nonlinearity.

position variation of the encoder output is 20–25 nm. Thus, it can be seen that the closed-loop positioning noise is reduced to the sensor noise.

In order to evaluate the tracking performance with the linear feedback controller, a 4 mm (i.e., 8 mm peak-to-peak), 2 Hz sinusoidal signal is applied as the command. The resulting tracking error was observed to be within ±46 μm, which is quite high for nanopositioning. A part of the tracking error comes from the phase error in the closed-loop transfer function at 2 Hz, which is approximately 0.6°. A lead-lag type feedforward compensator

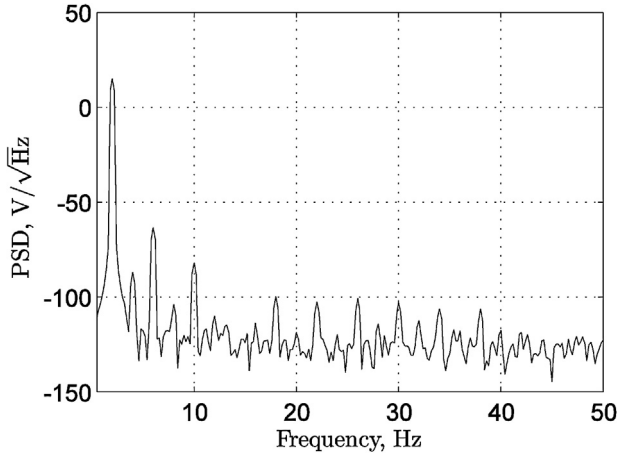


**Fig. 5.** Harmonic distortion in the actuator driver.

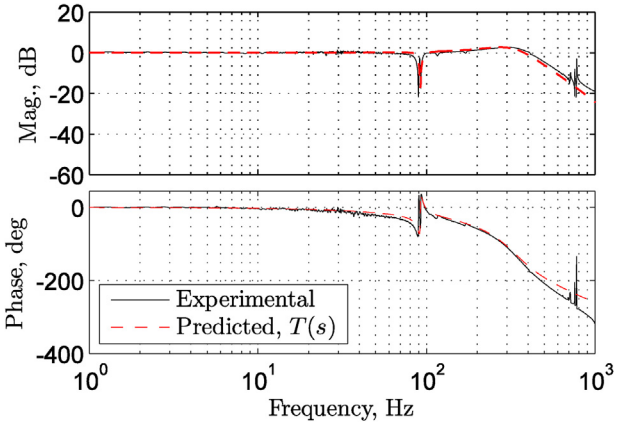


**Fig. 6.** Closed-loop frequency response.

$F(s)$ is added to correct for the phase error in the frequency range below 10 Hz. $F(s)$ is given by:

$$F(s) = \frac{3.807s + 3350}{s + 3350} \tag{3}$$

Fig. 8C shows the power spectrum of the tracking error with 0 dB corresponding to 1 $\mu m^2$/Hz. It is evident that the tracking error consists of broadband noise along with a component at the command signal frequency, as well as its higher harmonics. While the component at 2 Hz can be attributed to inadequate command following,

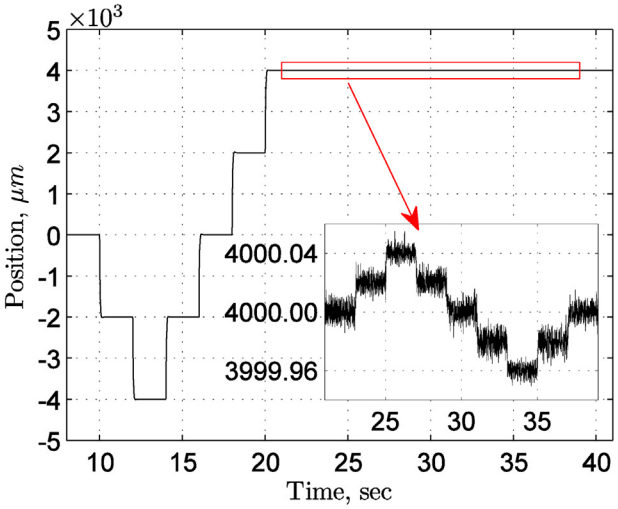


**Fig. 7.** Point-to-point positioning response.

Please cite this article in press as: Parmar G, et al. Large dynamic range nanopositioning using iterative learning control. Precis Eng (2013), http://dx.doi.org/10.1016/j.precisioneng.2013.07.003

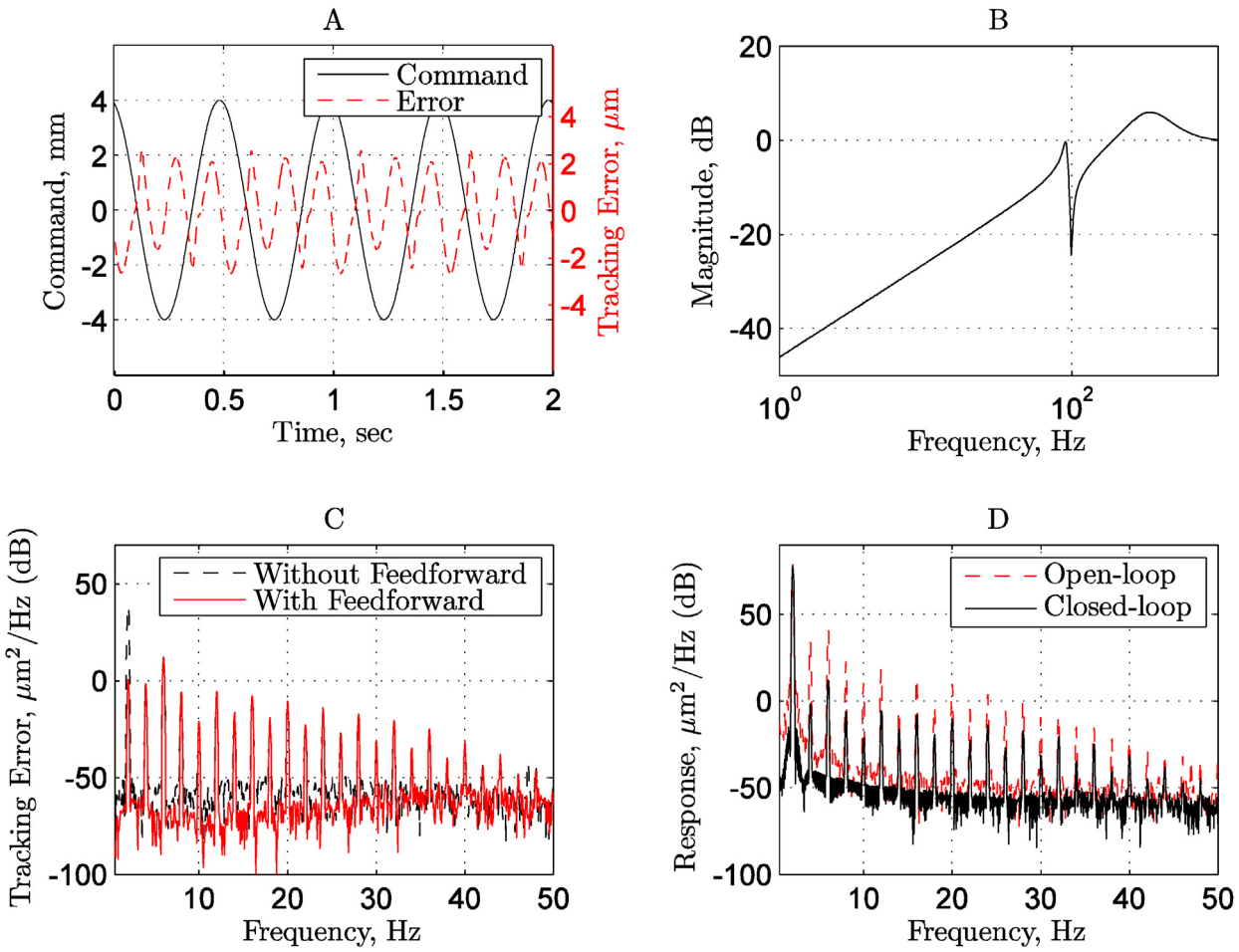


**Fig. 8.** Tracking performance with linear controller. (A) Position command and tracking error. (B) Sensitivity transfer function of the feedback loop. (C) Power spectrum of the tracking error. (D) Power spectrum of position response.

the higher frequency harmonics are a consequence of the nonlinearities in the actuator and the driver, as mentioned earlier. With the addition of the feedforward compensator, the tracking error is reduced to ±2.5 μm (see Fig. 8A). This corresponds to a reduction of about 18 times compared to performance obtained with feedback alone. This improvement comes only due to reduction of the tracking error at 2 Hz (see Fig. 8C). The fact that this error component is not fully eliminated can be attributed to the uncertainty in the closed loop transfer function model used to design the feedforward compensator. The higher frequency harmonics which originate due to the nonlinearities remain unaffected.

The feedback part of the linear controller does provide some reduction in the harmonic content as compared to tracking in an open-loop setting (see Fig. 8D). This reduction in the magnitude of the harmonics is a result of sensitivity reduction achieved due to feedback, and can be predicted by plotting the sensitivity transfer function. Fig. 8B shows the Bode magnitude plot of the sensitivity transfer function of the feedback loop. The harmonic component at 10 Hz, for example, is suppressed by 25 dB in closed-loop, corresponding to the −25 dB magnitude of the sensitivity transfer function. To achieve greater reduction of the harmonics, the sensitivity transfer function would have to be reduced further in the low frequency range. However, this can be done only at the cost of decreasing the stability robustness, given the actuator saturation concerns due to low open-loop bandwidth of the plant. This is a direct consequence of the analytic design tradeoff associated with the feedback loop, known as the *Bode waterbed effect* [34]. Hence, sensitivity reduction at low frequencies can only be achieved by increasing the lower bound on the peak of sensitivity function at intermediate frequencies, which results in loss of stability robustness.

From Fig. 8C, it can be seen that the deterministic part of the tracking error due to the nonlinearities as well as due to lack of command following is relatively large compared to the stochastic part due to various sources of noise and disturbance mentioned earlier. Moreover, if the command signal is periodic, then the deterministic part of the error also repeats every period. Therefore, in such cases, iterative learning control could be applied in conjunction with feedback in order to reduce the deterministic or the repeating portion of the tracking error [30,35]. This is done by modifying the control signal based on learning from the error histories obtained during previous iterations.

## 4. Iterative learning control: design and implementation

The ILC block diagram incorporated with the feedback loop in shown in Fig. 9. Here, $P$, $C$, and $F$ denote the plant, the feedback compensator, and the feedforward compensator, respectively. $y_d(k)$ is a periodic command signal and $y(k)$ is the measured response. The objective of ILC is to generate a feedfoward command $u(k)$ in order to reduce the tracking error $e(k) = y_d(k) - y(k)$. The tracking error $e_j(k)$ and the ILC input $u_j(k)$ are stored in a memory for every iteration $j$ and time instant $k$. The ILC algorithm then evaluates the new input signal, $u_{j+1}(k)$, in an offline manner, to be applied during the

Please cite this article in press as: Parmar G, et al. Large dynamic range nanopositioning using iterative learning control. Precis Eng (2013), http://dx.doi.org/10.1016/j.precisioneng.2013.07.003

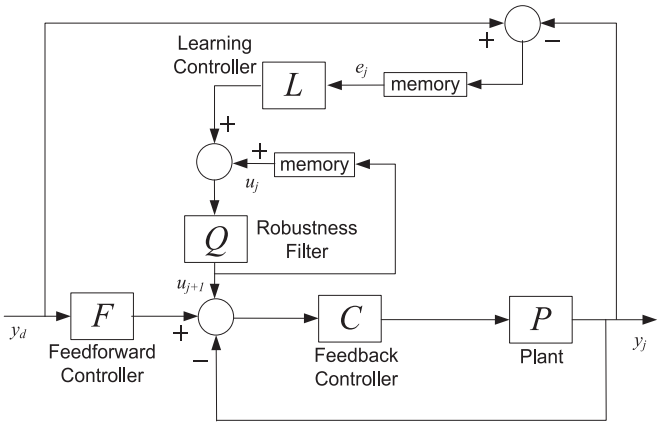


**Fig. 9.** Iterative learning control architecture.

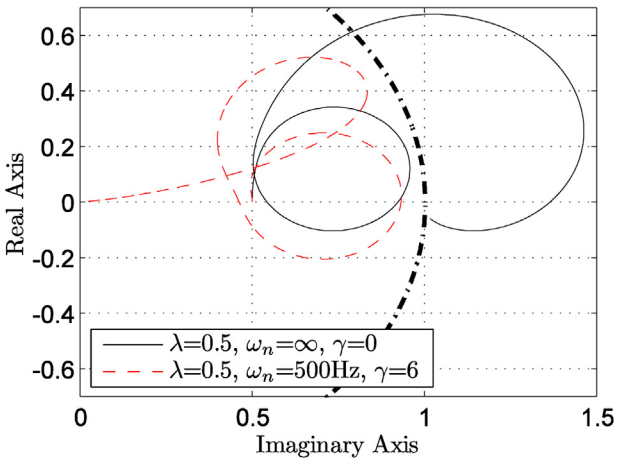


**Fig. 10.** Nyquist plot for monotonic convergence criterion.

next iteration. The iteration period can be chosen as the command period or any multiple of the command period. The arrangement shown is also known as the serial ILC architecture because the ILC input is added to the command before the feedback loop. Although a serial architecture is chosen here, a similar analysis and design procedure, as shown below, could be followed to implement an equivalent parallel ILC architecture [35].

A first-order classical ILC update law is given as follows [30]:

$$u_{j+1}(k) = Q(z)[u_j(k) + L(z)e_j(k)] \tag{4}$$

where $L$ and $Q$ are known as the learning filter and robustness filter, respectively. The design of these filters determines the performance and the robustness of the ILC algorithm as described next [35,36].

With the assumption that the feedback loop is stable and linear time-invariant, a sufficient condition guaranteeing stability and monotonic convergence of the tracking error in successive iterations is given by the following standard frequency-domain result:

$$\left|Q(z)[1 - L(z)T(z)]\right| < 1, \quad z = e^{i\omega T} \quad \forall\omega \tag{5}$$

where $T(z)$ represents the $z$-transform of the closed-loop transfer function. The error dynamics is given by the following relation:

$$(e_\infty(k) - e_{j+1}(k)) = Q(1 - LT)(e_\infty(k) - e_j(k)) \tag{6}$$

Additionally, it can be shown that, given the initial tracking error, $e_0(t)$, the tracking error finally converges to

$$e_\infty(k) = \frac{1 - Q}{1 - Q(1 - LT)} e_0(k) \tag{7}$$

From Eq. (6), it can be deduced that the learning filter determines the rate of convergence of tracking error in successive iterations. Specifically, the magnitude of $(1 - LT)$ should be small for fast convergence. Since the closed-loop transfer function $T$ is designed to have unity magnitude up to a frequency range of approximately 400 Hz (see Fig. 6), $L$ can be simply chosen as $L(z) = \lambda z^\gamma$ with $\lambda \leq 1$ as a constant gain and $\gamma > 0$ representing the linear phase lead, resulting in a linear phase lead type iterative learning controller [30]. While higher values of $\lambda$ leads to aggressive learning, smaller gains makes the learning process less sensitive to noise and leads to lower final errors. Also, because $\lambda$ is a constant gain, it can be easily tuned online while performing experiments. Secondly, $\gamma > 0$ is chosen to satisfy the stability criterion as described next, resulting in a non-causal transfer function. However, its implementation is not an issue because the ILC computation is performed retrospectively once per trajectory repetition.

The robustness filter $Q$ is usually chosen to be a low pass filter with the bandwidth ($\omega_n$) of $Q$ presenting a trade-off between performance and robustness. As seen from Eq. (7), choosing $Q$ as unity ensures convergence to zero tracking error. The Nyquist plot of $Q(1 - LT)$ for $\lambda = 0.5$, $\gamma = 0$ and $Q = 1$ is shown in Fig. 10. The plot goes outside the unit circle at the frequency of about 280 Hz, thereby violating the monotonic convergence criterion given in Eq. (5). The phase lead $z^\gamma$ can be used to increase the bandwidth of the $Q$ filter. Also plotted in Fig. 10 is the Nyquist plot of $Q(1 - LT)$ for $\lambda = 0.5$, $\omega_n = 500$ Hz, and $\gamma = 6$. The curve remains within unit circle over the entire frequency range with the maximum value of $|Q(1 - LT)|$ being 0.93. Simulation conducted showed that the overall system remains stable for the plant gain variation up to 45%. The $Q$ filter is designed as a 5th order Butterworth filter to obtain a sharp cut-off. Moreover, since the filtering is done in an offline manner, $Q$ is designed to be non-causal, using the *filtfilt* function in Matlab. The *filtfilt* function performs signal filtering in both the forward and reverse directions, resulting in zerophase error in the filtered signal [33].

Fig. 11 shows the scheme adopted for the implementation of the ILC. The error signal $e_{j-1}(k)$ and the ILC input signal $u_{j-1}(k)$ are stored in a memory buffer during the $(j-1)$th iteration. The buffers already contain signal values from previous two iterations as shown. During iteration $j$, these buffers are then used to compute the ILC control signal for $(j+1)$th iteration according to the following modified ILC law:

$$u_{j+1}(k) = Q[u_{j-2}(k) + Le_{j-2}(k)] \tag{8}$$

The resultant ILC control input $u_{j+1}(k)$ is then unbuffered and applied to the feedback loop during the $(j+1)$th iteration. The memory buffers contain signal values for 3 iterations in order to facilitate non-causal filtering by taking into account the filter initial conditions. It should be noted that while the feedback computations are done at the sampling rate, the ILC calculation is carried out only once during an iteration.

## 5. Experimental results

The combined feedback and ILC controller described above was applied to the single-axis nanopositioning system. Fig. 12 shows the resulting tracking performance for a 4 mm amplitude (i.e., 8 mm peak-to-peak), 2 Hz sinusoidal command. Based on the ILC design described earlier, the learning gain ($\lambda$), phase lead parameter ($\gamma$), and $Q$ filter bandwidth ($\omega_n$) were set to 0.5, 6 and 500 Hz, respectively. Fig. 12A shows the decrease in the tracking error as a function of the iteration number. The RMS of the tracking error is reduced from about 1.8 μm to 10 nm in approximately 40 iterations. This corresponds to a reduction by a factor of about

Please cite this article in press as: Parmar G, et al. Large dynamic range nanopositioning using iterative learning control. Precis Eng (2013), http://dx.doi.org/10.1016/j.precisioneng.2013.07.003

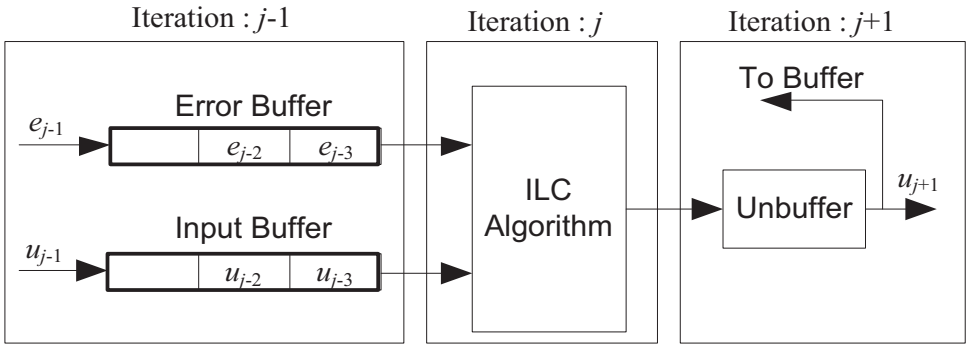


**Fig. 11.** ILC offline implementation.

180 in 20 s. The tracking error at the end of the 40th iteration is plotted in Fig. 12B. The performance improvement, compared to linear controller by itself, comes from a reduction in the repeating portion of the tracking error at the command frequency and its harmonics (Fig. 12D). The ILC input follows a profile similar to the tracking error, because of the use of constant gain type learning controller. The dynamic range of the nanopositioning system, defined as the ratio of the RMS command (2.83 mm) to that of the RMS tracking error (10 nm), is equal to $2.83 \times 10^5$. The power spectrum of the converged position response, shown in Fig. 12C, reflects the true dynamic range of the nanopositioning system.

In a separate experiment, a 4 mm and 2 Hz band-limited triangular waveform was applied as the command. The signal was optimized to have a perfectly linear (constant velocity) region within ±2 mm while minimizing the power content beyond the first three harmonics [37]. The motion speed in the linear region is 32 mm/s. As compared to sinusoids, multi-tone command signals are more challenging to follow since they give rise to the intermodulation products in addition to the harmonics. Even in this case, the tracking error after 40 iterations (Fig. 13A) is reduced to 10 nm (RMS). The power spectrum of the measured response and the tracking error are shown in Fig. 13B.

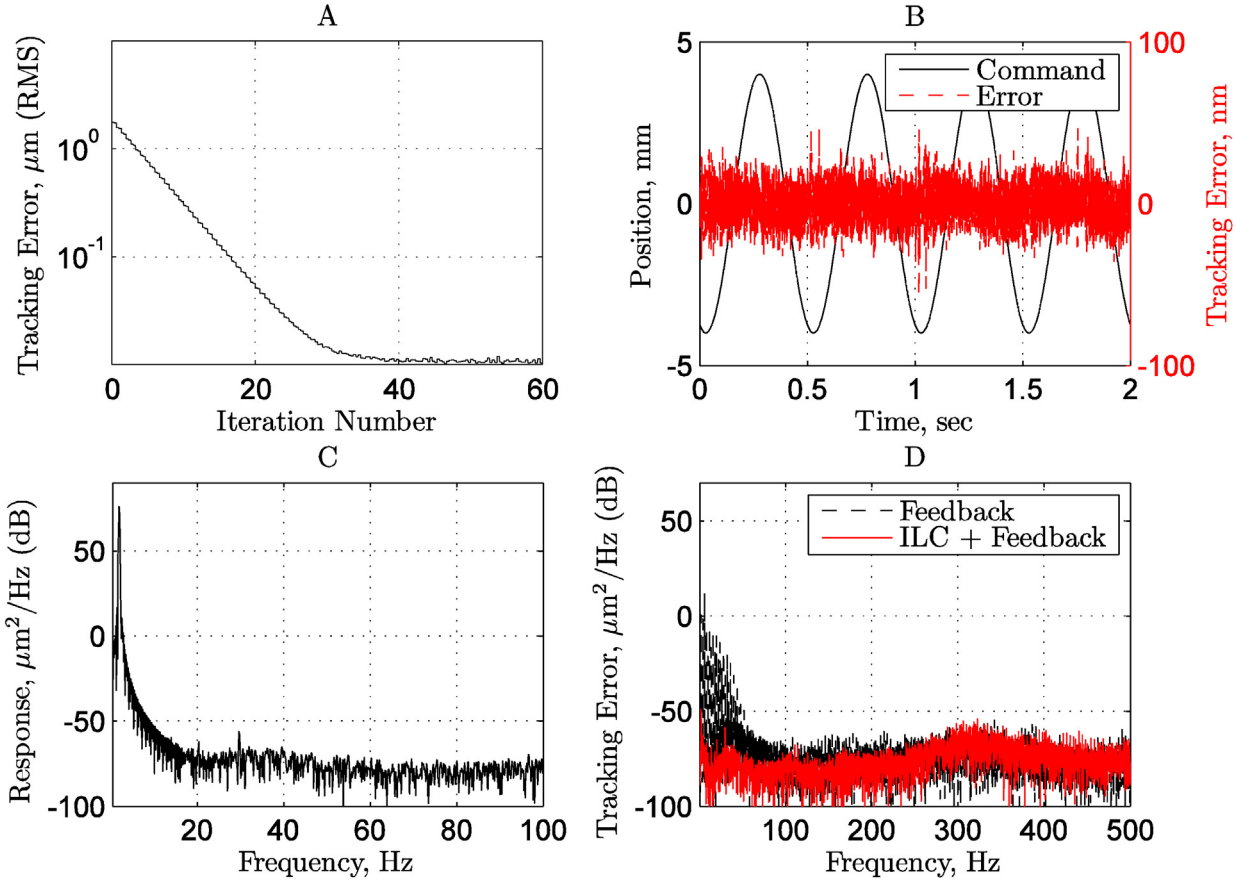


**Fig. 12.** Tracking performance with combined feedback and ILC. (A) Tracking error convergence. (B) Position command and tracking error after 40 iterations. (C) Power spectrum of position response. (D) Power spectrum of tracking error.

Please cite this article in press as: Parmar G, et al. Large dynamic range nanopositioning using iterative learning control. Precis Eng (2013), http://dx.doi.org/10.1016/j.precisioneng.2013.07.003

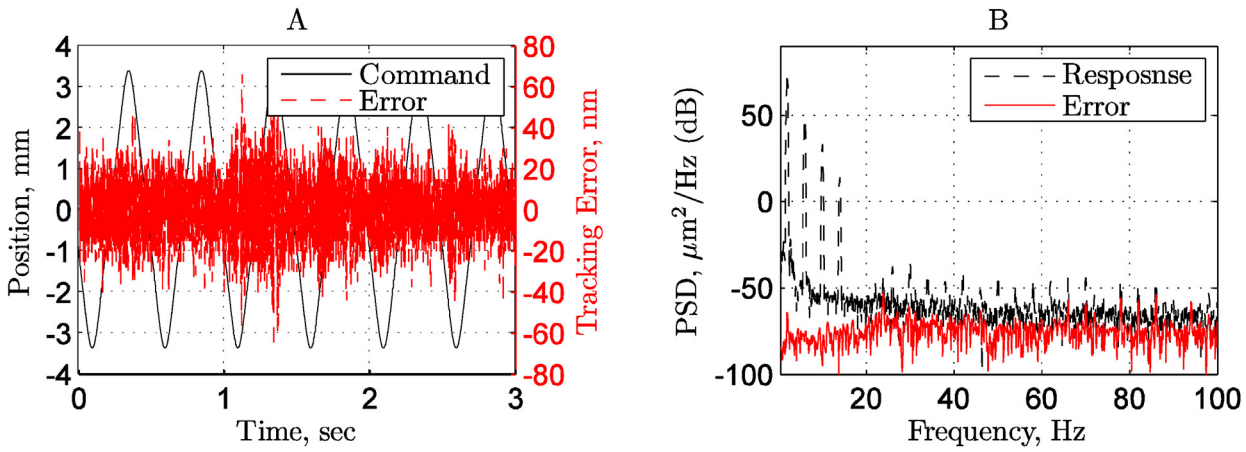


**Fig. 13.** Tracking performance for an optimized triangular command. (A) Time response. (B) Power spectrum.

## 6. Conclusion

In this paper, an iterative learning controller is applied to improve the tracking performance of a large range single-axis nanopositioning system. In case of periodic commands, the non-linearities in the moving magnet actuator as well as in the actuator driver produce deterministic and repeating error. While linear feedback alone proves to be inadequate, a phase lead type serial-architecture iterative learning controller in conjunction with the linear feedback and feedforward controller is shown to reduce the tracking error by more than two orders of magnitude. The experimental results show potential of flexure bearing and moving magnet actuator based nanopositioning systems for simultaneously achieving large range, high speed, and nanometric motion quality. The only drawback of ILC is that it works only for repetitive or periodic commands, which is acceptable for the targeted scanning-type applications. The resultant tracking error is approximately 2 times larger than the sensor resolution, leaving some scope for further improvement. In future, other choices of learning filters [35] along with averaging of the ILC input [38] will be investigated to further reduce the tracking error as well as to improve the rate of convergence.

## Acknowledgements

This work was supported in part by a National Science Foundation Grant (CMMI # 1100807). The first author also acknowledges a Measurement Science and Engineering Fellowship from the National Institute of Science and Technology.

## References

[1] Devasia S, Eleftheriou E, Moheimani SOR. A survey of control issues in nanopositioning. IEEE Transactions on Control Systems Technology 2007;15:802–23.
[2] Awtar S, Parmar G. Design of a large range XY nanopositioning system. In: ASME international design engineering technical conference. 2010. p. 387–99.
[3] O'Brien W. Long-range motion with nanometer precision. Photonics Spectra 2005;39:80–1.
[4] Sinno A, Ruaux P, Chassagne L, Topcu S, Alayli Y, Lerondel G, et al. Enlarged atomic force microscopy scanning scope: novel sample-holder device with millimeter range. Review of Scientific Instruments 2007;78:095107–95117.
[5] Salaita K, Wang Y, Mirkin CA. Applications of dip-pen nanolithography. Nature Nanotechnology 2007;2:145–55.
[6] Madou MJ. Fundamentals of microfabrication: the science of miniaturization. Boca Raton: CRC Press; 2002.
[7] Kramar JA. Nanometre resolution metrology with the molecular measuring machine. Measurement Science and Technology 2005;16:2121.
[8] Maeda GJ, Sato K. Practical control method for ultra-precision positioning using a ballscrew mechanism. Precision Engineering 2008;32:309–18.
[9] Chassagne L, Wakim M, Xu S, Topcu S, Ruaux P, Juncar P, et al. A 2D nanopositioning system with sub-nanometric repeatability over the millimetre displacement range. Measurement Science and Technology 2007;18:3267–72.
[10] Lihua L, Yingchun L, Yongfeng G, Akira S. Design and testing of a nanometer positioning system. Journal of Dynamic Systems, Measurement, and Control 2010;132:021011–21016.
[11] Buice ES, Otten D, Yang RH, Smith ST, Hocken RJ, Trumper DL. Design evaluation of a single-axis precision controlled positioning stage. Precision Engineering 2009;33:418–24.
[12] Choi Y-M, Jung Jae K, Jinwoo K, Dae-Gab G. Design and control of a nanoprecision XY scanner. Review of Scientific Instruments 2008;79:045109–45111.
[13] Zschaeck S, Amthor A, Ament C. Decentralized high precision motion control for nanopositioning and nanomeasuring machines. In: 37th annual conference on IEEE industrial electronics society. 2011. p. 546–51.
[14] Michellod Y, Mullhaupt P, Gillet D. Strategy for the control of a dual-stage nanopositioning system with a single metrology. In: IEEE conference on robotics, automation and mechatronics. 2006. p. 1–8.
[15] Kosinskiy M, Liu Y, Ahmed SIU, Scherge M, Schafer JA. Tribology of nanopositioning characterization of precision linear bearings on nanometre scale. VDI Berichte 2006:215–24.
[16] Holmes M, Hocken R, Trumper D. Long-range scanning stage: a novel platform for scanned-probe microscopy. Precision Engineering 2000;24:191–209.
[17] Kim W-J, Verma S. Multiaxis maglev positioner with nanometer resolution over extended travel range. Transactions of the ASME Journal of Dynamic Systems, Measurement and Control 2007;129:777–85.
[18] Khan MU, Bencheikh N, Prelle C, Lamarque F, Beutel T, Buttgenbach S. A long stroke electromagnetic XY positioning stage for micro applications. IEEE/ASME Transactions on Mechatronics 2011:1–10.
[19] Dejima S, Wei G, Katakura K, Kiyono S, Tomita Y. Dynamic modeling, controller design and experimental validation of a planar motion stage for precision positioning. Precision Engineering 2005;29:263–71.
[20] Shinno H, Hashizume H, Yoshioka H, Komatsu K, Shinshi T, Sato K. $X$–$Y$–$\theta$ nanopositioning table system for a mother machine. CIRP Annals – Manufacturing Technology 2004;53:337–40.
[21] Maeda GJ, Sato K, Hashizume H, Shinshi T. Control of an XY nano-positioning table for a compact nano-machine tool. JSME International Journal, Series C (Mechanical Systems, Machine Elements and Manufacturing) 2006;49:21–7.
[22] Hesse S, Schaffel C, Mohr HU, Katzschmann M, Buchner HJ. Design and performance evaluation of an interferometric controlled planar nanopositioning system. Measurement Science & Technology 2012;23:074011 (10 pp).
[23] Kang D, Kim K, Kim D, Shim J, Gweon D-G, Jeong J. Optimal design of high precision XY-scanner with nanometer-level resolution and millimeter-level working range. Mechatronics 2009;19:562–70.
[24] Fukada S, Nishimura K. Nanometric positioning over a one-millimeter stroke using a flexure guide and electromagnetic linear motor. International Journal of Precision Engineering and Manufacturing 2007;8:49–53.
[25] Aoyama T, Koizumi K, Kakinuma Y, Kobayashi Y. Numerical and experimental analysis of transient state micro-bounce of aerostatic guideways caused by small pores. CIRP Annals – Manufacturing Technology 2009;58:367–70.
[26] Chen X, Chen H, Luo X, Ye Y, Hu Y, Xu J. Air vortices and nano-vibration of aerostatic bearings. Tribology Letters 2011;42:179–83.
[27] Awtar S, Ustick J, Sen S. An XYZ parallel kinematic flexure mechanism with geometrically decoupled degrees of freedom. In: ASME international design engineering technical conference. 2011. p. 119–26.
[28] Butler H. Position control in lithographic equipment. Control Systems, IEEE 2011;31:28–47.
[29] Parmar G, Hiemstra D, Chen Y, Awtar S. A moving magnet actuator for large range nanopositioning. In: ASME dynamic systems and control conference. 2011. p. 41–8.
[30] Longman RW. Iterative learning control and repetitive control for engineering practice. International Journal of Control 2000;73:930–54.

Please cite this article in press as: Parmar G, et al. Large dynamic range nanopositioning using iterative learning control. Precis Eng (2013), http://dx.doi.org/10.1016/j.precisioneng.2013.07.003

[31] Otten G, de Vries TJA, van Amerongen J, Rankers AM, Gaal EW. Linear motor motion control using a learning feedforward controller. IEEE/ASME Transactions on Mechatronics 1997;2:179–87.
[32] Steinbuch M, Molengraft MJGVD. Iterative learning control of industrial motion systems. In: 1st IFAC conference on mechatronic systems. 2000. p. 967–72.
[33] Signal processing Toolbox™ user's guide. MathWorks Inc. http://www.mathworks.com/help/pdf_doc/signal/signal_tb.pdf
[34] Freudenberg JS, Looze DP. Frequency domain properties of scalar and multivariable feedback systems 70. Berlin: Springer-Verlag; 1988.
[35] Bristow DA, Tharayil M, Alleyne AG. A survey of iterative learning control. IEEE Control Systems Magazine 2006;26:96–114.
[36] Norrlöf M, Gunnarsson F. Time and frequency domain convergence properties in iterative learning control. International Journal of Control 2002;75:1114–26.
[37] Fleming AJ, Wills AG. Optimal periodic trajectories for band-limited systems. IEEE Transactions on Control Systems Technology 2009;17:552–62.
[38] Merry R, van de Molengraft R, Steinbuch M. Removing non-repetitive disturbances in iterative learning control by wavelet filtering. In: American control conference. 2006, 6 pp.

Please cite this article in press as: Parmar G, et al. Large dynamic range nanopositioning using iterative learning control. Precis Eng (2013), http://dx.doi.org/10.1016/j.precisioneng.2013.07.003